Nanoplasmonic biosensing with focus on short-range ordered nanoholes in thin metal films (Review)

Magnus P. Jonsson[a] and Andreas B. Dahlin
Department of Applied Physics, Chalmers University of Technology, SE-41296 Gothenburg, Sweden

Peter Jönsson
Division of Solid State Physics, Lund University, SE-22100 Lund, Sweden

Fredrik Höök[b]
Department of Applied Physics, Chalmers University of Technology, SE-41296 Gothenburg, Sweden

(Received 11 July 2008; accepted 21 October 2008; published 28 January 2009)

The resonance conditions for excitation of propagating surface plasmons at planar metal/dielectric interfaces and localized surface plasmons associated with metal nanostructures are both sensitive to changes in the interfacial refractive index. This has made these phenomena increasingly popular as transducer principles in label-free sensing of biomolecular recognition reactions. In this article, the authors review the recent progress in the field of nanoplasmonic bioanalytical sensing in general, but set particular focus on certain unique possibilities provided by short-range ordered nanoholes in thin metal films. Although the latter structures are formed in continuous metal films, while nanoparticles are discrete entities, these two systems display striking similarities with respect to sensing capabilities, including bulk sensitivities, and the localization of the electromagnetic fields. In contrast, periodic arrays of nanoholes formed in metal films, most known for their ability to provide wavelength-tuned enhanced transmission, show more similarities with conventional propagating surface plasmon resonance. However, common for both short-range ordered and periodic nanoholes formed in metal films is that the substrate is electrically conductive. Some of the possibilities that emerge from sensor templates that are both electrically conductive and plasmon active are discussed and illustrated using recent results on synchronized nanoplasmonic and quartz crystal microbalance with dissipation monitoring of supported lipid bilayer formation and subsequent biomolecular recognition reactions. Besides the fact that this combination of techniques provides an independent measure of biomolecular structural changes, it is also shown to contribute with a general means to quantify the response from nanoplasmonic sensors in terms of bound molecular mass. © *2008 American Vacuum Society.* [DOI: 10.1116/1.3027483]

I. INTRODUCTION

Under certain conditions the interaction of light with metal structures results in the excitation of propagating and/or localized surface plasmons, which are both collective oscillations of the free electrons in the metal. The significant research efforts currently undertaken on studies of these phenomena are motivated by the huge potential of plasmonic devices foreseen in diverse areas such as solar cells,[1] light emitting diodes,[2] bioimaging,[3] and both medical diagnostics[4] and therapy.[5] The growing interest in different aspects of plasmonics also stems from a combination between the rapid development of advanced top-down and bottom-up nanofabrication techniques[6] and the progress recently made with respect to theoretical representations of the optical properties of nanoscale metal objects.[7–10] The fabrication is generally made using either wet-chemical synthesis or surface-based lithography methods or a combination of these. While the former method is best suited for production of suspended metal nanoparticles with controlled sizes and shapes, and thus with variable plasmonic properties,[11–14] the latter concept provides controlled spatial distribution of surface-attached nanoparticles,[6,15,16] including fabrication of sandwiched structures.[17] In combination with, for example, material-specific surface chemistries, the combination of the two can also be used to control the positioning of suspended nanoparticles on nanofabricated substrates.[18] Furthermore, surface-based lithography methods can be used to fabricate continuous metal structures that display plasmonic properties, such as nanometer-sized apertures in both optically transparent and opaque metal films.[19,20] A detailed account on the fabrication of the most common nanoplasmonic structures can be found in the recent review by Stewart *et al.*[21]

With focus on applications in the field of bioanalytical sensing, we review in this article the optical properties of different plasmonic structures, including (i) planar metal films, (ii) metal films perforated with periodic nanoholes, (iii) discrete metal nanoparticles, and (iv) short-range ordered nanoholes in metal films [the short-range order is referred to as a structure without long-range periodic order, but with a narrow nearest-neighbor distance distribution (Ref. 15)], with particular focus on the latter structure, and refer to recent reviews by others[21–25] for detailed accounts on the former structures. The prime aim of this article is to address

[a]Electronic mail: magnus.p.jonsson@chalmers.se
[b]Electronic mail: fredrik.hook@chalmers.se

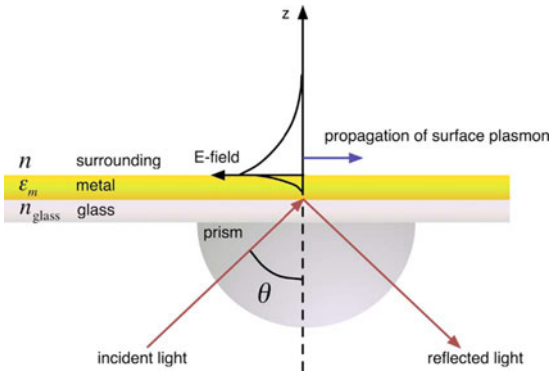

FIG. 1. Schematic illustration of the excitation of propagating SPPs.

features and potentials that are common irrespective of which nanostructure that is utilized and also to discuss applications that are unique for certain structures. While periodic arrays of nanoholes have been shown to display certain similarities with conventional grating-coupled propagating surface plasmon resonance (SPR),[26] nanoparticles and short-range ordered nanoholes both display plasmonic fields that are highly localized to the particle or the void of the holes, respectively.[20,27] However, there are also significant differences between the latter two structures, which may have strong implications on their potential use as transducer elements in bioanalytical sensors. In their use as traditional affinity sensors, in which case biorecognition reactions are detected by recording the colorimetric changes of the sensor elements induced upon changes in interfacial refractive index, there is no principle difference between the two systems. The method of choice should rather be determined from the sensitivity, simplicity of fabrication, preferred surface modification, and robustness. Discrete nanoparticles, however, can be suspended in solution, which may be beneficial in some applications, where sensing within living cells is one recent example.[28] On the other hand, the continuity of metal films perforated with nanoholes provides a unique opportunity for combining nanoplasmonic sensing with other transducer formats that rely on electrical readout. These aspects, which are of outmost importance depending on the systems under investigation, are addressed with suitable examples from us and others, with focus on the use of nanoplasmonic sensors to analyze biomolecular structural changes and means to quantify the response from nanoplasmonic sensors in terms of bound molecular mass.

II. CONVENTIONAL SURFACE PLASMON RESONANCE

Propagating surface plasmons, often denoted surface plasmon polaritons (SPPs), are electromagnetic waves bound to a metal surface. When excited, these waves propagate at the interface between the metal and a dielectric material (see schematic illustration in Fig. 1) with typical propagation lengths on the order of tens of micrometers.[29] The electromagnetic field associated with SPPs decays exponentially from the metal surface with a decay length on the order of hundreds of nanometers.[29] The wave vector, k_{SPP}, of SPPs with angular frequency ω depends on the dielectric function of the metal, ε_m, at that frequency and the refractive index of the surrounding medium, n, according to the dispersion relation[30]

$$k_{SPP} = \frac{\omega}{c}\sqrt{\frac{\varepsilon_m n^2}{\varepsilon_m + n^2}}, \tag{1}$$

where c is the speed of light in vacuum. For a photon traveling in a medium with refractive index n_2 the component of the wave vector that is parallel to a planar metal/dielectric interface is

$$k_{photon} = \frac{\omega}{c} n_2 \sin\theta, \tag{2}$$

where θ is the incidence angle (see Fig. 1). A comparison between Eqs. (1) and (2) shows that photons incident from the sensing side of the device ($n_2 = n$) cannot excite SPPs because the dispersion relation of these photons do not coincide with that of the surface plasmons (ε_m is negative). In other words, irrespective of wavelength, there are no angles of incidence at which both the frequency (energy) and the wave vector (momentum) of photons and SPPs are matched. This can be circumvented by exciting SPPs with light guided via a glass prism ($n_2 = n_{glass}$) in optical contact with the back of a sample. In this setup, called the Kretschmann configuration (see Fig. 1),[31] the incidence angle of the light at a given wavelength can be tuned to fulfill the resonance condition according to

$$\theta = \arcsin\left(\frac{n}{n_{glass}}\sqrt{\frac{\varepsilon_m}{\varepsilon_m + n^2}}\right). \tag{3}$$

Alternatively, using white light incident at a given angle, SPPs are excited at a unique wavelength.

Equation (3) shows that the resonance condition for excitation of SPPs is dependent on the refractive index of the surrounding medium. In a pioneering work by Liedberg *et al.*[30] this was utilized to monitor antigen-antibody binding reactions on a silver surface in real time. After the report of the first SPR biosensor, several commercial systems have been developed and are today widely used worldwide. Although they will not be further discussed herein, it is worth mentioning that several extensions of the concept have been developed, including imaging SPR,[32,33] providing real-time measurements of biorecognition reactions with down to 100 μm resolution, and surface plasmon-enhanced fluorescence spectroscopy.[34]

As evident from Eqs. (1) and (2) light at normal incidence have no momentum parallel to the surface and cannot excite SPPs at a planar metal/dielectric interface. Still, working at normal incidence would significantly simplify the experimental setup and indeed this can be accomplished by coupling the light using a grating on the metal surface.[23,35,36] At normal incidence light diffracted by the grating can then obtain a momentum component that is parallel to the metal film according to[23]

$$k_{\text{photon}} = \frac{i2\pi}{P}, \tag{4}$$

where P is the lattice constant and i is a nonzero integer number representing the scattering orders from the grating. Using $\omega = 2\pi c/\lambda$ and combining Eqs. (1) and (4) it is revealed that there will be a match between both the momentum and the energy of the photons and the SPPs at a wavelength, λ_{peak}, according to

$$\lambda_{\text{peak}} = \frac{P}{i}\sqrt{\frac{\varepsilon_m n^2}{\varepsilon_m + n^2}}. \tag{5}$$

As shown below, the resonance condition shown in Eq. (5) is indeed very similar to those of periodic arrays of nanoholes, which have recently shown great promise in various biosensor applications.

III. PERIODIC ARRAYS OF NANOHOLES

In analogy with grating-coupled SPR, propagating plasmons can also be excited at normal incidence utilizing the diffraction of light in a metal film perforated with a periodic array of apertures. For a square array of nanoholes the value of the momentum component of light parallel to the surface can be described by[37]

$$k_{\text{photon}} = \frac{2\pi}{P}\sqrt{i^2 + j^2}, \tag{6}$$

where P again is the lattice constant (the distance between the nanoholes in this case) and i and j are nonzero integer numbers representing the scattering orders from the two-dimensional array. Hence, following the reasoning above, SPPs can then, to a first approximation, be excited at peak positions that satisfy[26,38,39]

$$\lambda_{\text{peak}} = \frac{P}{\sqrt{i^2 + j^2}}\sqrt{\frac{\varepsilon_m n^2}{\varepsilon_m + n^2}}. \tag{7}$$

For simplicity reasons, the wavelength dependence of ε_m is not explicitly included. However, as described below this dependence is essential in the use of localized surface plasmons for refractive index based sensing.

For an opaque metal film perforated with a periodic array of nanoholes, light at wavelengths satisfying Eq. (7) can be transmitted at intensities that are orders of magnitude larger than those predicted from classical aperture optics.[22,37,38] Such enhanced, or extraordinary transmission, is illustrated in Fig. 2, which also shows how the wavelength at maximum transmission depends on the period of the array, as evident from Eq. (7).[40] It is also clear from Eq. (7) that the peak position will change in response to a change in the refractive index of the bulk medium[41] and in agreement with grating-coupled SPR sensors, it has been shown that periodic nanohole arrays have bulk sensitivities on the order of hundreds of nanometers per refractive index unit (RIU) at visible wavelengths.[26,29] Brolo *et al.*[26] utilized this feature to probe interfacial refractive index changes induced by binding of biomolecules to the surface of a periodic gold nanohole array

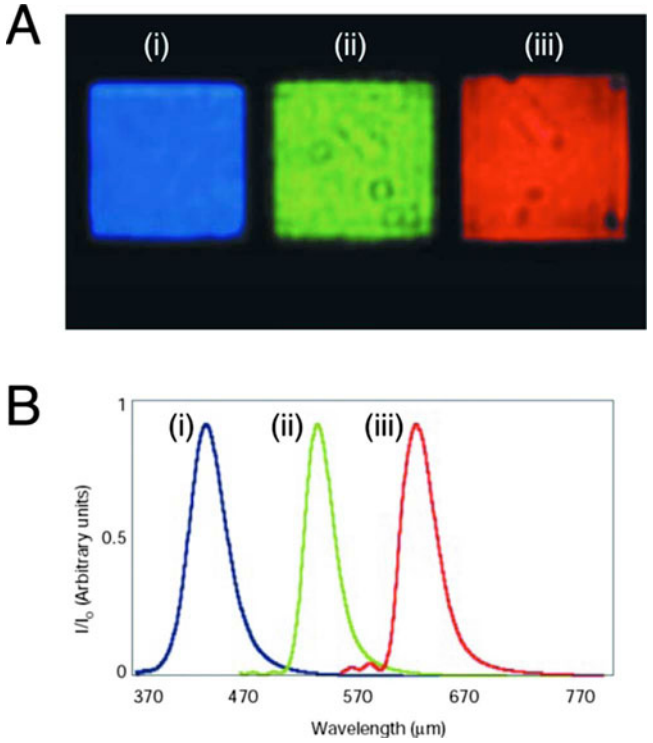

FIG. 2. Transmission at normal incidence through arrays of nanoholes in a freestanding 300 nm thick silver film with periods (i) 300 nm, (ii) 450 nm, and (iii) 550 nm. The hole diameters are (i) 155 nm, (ii) 180 nm, and (iii) 225 nm. (A) shows transmission images and (B) are the corresponding transmission spectra. From Barnes *et al.*, Nature (London), 2003. Reprinted by permission of Macmillan Publishers Ltd.

by measuring changes in the peak position of the transmission spectrum. Later, the concept was extended to, for example, real-time sensing and spatially resolved biosensing using two similar multilayer metal nanostructures (Fig. 3).[39,42] The first of these quasi-three-dimensional plasmonic crystals were fabricated by evaporation of gold on top of a polymer layer with a periodic array of nanoholes, which results in a perforated metal layer with a gold disk in the bottom of each hole.[39] The latter structure, from which the results in Fig. 3 were obtained, was produced using metal sputtering instead of evaporation, resulting in deposition of metal also on the side walls of the nanowells and a completely continuous structure [see Fig. 3(A)].[42]

Some features of the transmission spectra of both of these structures can be associated with localized surface plasmons (see further below), which is also considered to play a central a role in the enhanced transmission through conventional periodic nanohole arrays.[43] However, due to the large diffractive coupling from the periodicity of the arrays, effects from excitation of propagating SPPs have been found to dominate.[39,43] The corresponding decay lengths are therefore similar to conventional SPR sensors and are on the order of hundreds of nanometers.[26,39] This is about one order of magnitude longer than typical decay lengths associated with both discrete plasmon active nanostructures and short-range ordered nanoholes in thin metal films. As discussed below, this

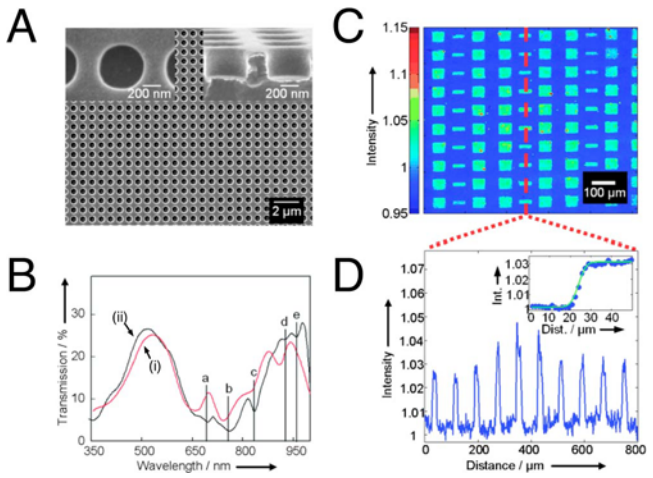

FIG. 3. (A) Scanning electron microscopy images of a three-dimensional plasmonic crystal presented by Yao *et al.* (Ref. 42). The left inset is a high-magnification top view and the right inset is an image of the structure at a high angle and shows the continuous gold layer on the surface of the nanowell array. (B) Normal-incidence transmission spectrum of a plasmonic crystal in water (i) and corresponding rigorous electrodynamics modeling of the spectrum (iii). (a)–(g) represent transmission peaks corresponding to both localized and propagating plasmons. (C) Transmitted-light images of arrays of squares and rectangles consisting of monolayers of 1-octadecanethiol on a plasmonic crystal. (D) Vertical line profile through the image in (C). The inset shows a measured step edge (symbols) and a fitted step edge (full line) with a Gaussian width of 3 μm. From Yao *et al.*, Angewandte Chemie, International Edition, 2008. Reprinted with permission of Wiley-VCH Verlag GmbH & Co. KGaA.

is an important difference that should be carefully considered when these types of sensors are designed for specific applications.

IV. DISCRETE NANOPARTICLES

In a discrete metal nanoparticle there is no space for SPPs to propagate. However, local collective oscillations of the free electrons can be excited at specific resonance wavelengths, as schematically illustrated in Fig. 4. These plasmons are therefore referred to as localized surface plasmons (LSPs). Although the concept of localized surface plasmon resonance (LSPR) is younger than conventional SPR with respect to sensing applications, the optical properties of metal nanoparticles were utilized already in the medieval times, when gold and silver colloids were used to create beautiful colors in, e.g., church windows. In analogy with the excitation of propagating SPPs on planar metal films, the resonance condition for excitation of LSPs is also sensitive

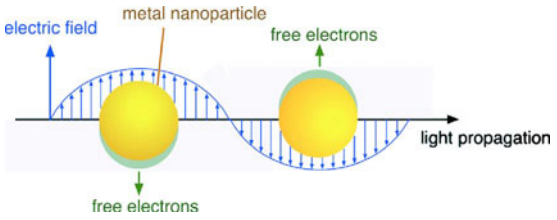

FIG. 4. Illustration of the excitation of localized surface plasmons in nanoparticles.

to the refractive index of the surrounding medium in close proximity to the nanostructure. Hence, the base for using the LSPR phenomenon for sensing applications is essentially the same as that of SPR. In analogy with grating- or periodic nanohole-coupled excitation of SPPs, LSPs can be excited by light at normal incidence. For example, color changes in LSPR active nanostructures induced by changes in the surrounding medium can be probed in transmission mode using ordinary spectrophotometers. This, together with the simplicity by which these structures can be fabricated and the potential they have with respect to miniaturization, is the prime reason behind the belief that LSPR sensors have a great potential to replace other label-free bioanalytical sensors.

The optical cross section of a metal nanosphere was derived already 100 hundred years ago by Mie, and in the electrostatic dipole limit it can be expressed as[44]

$$\sigma(\lambda) = \frac{18\pi V}{\lambda} n^3 \frac{\varepsilon_i(\lambda)}{(\varepsilon_r(\lambda) + 2n^2)^2 + \varepsilon_i(\lambda)^2}, \tag{8}$$

where V is the volume of the sphere and n is the refractive index of the surrounding medium. The real and imaginary parts of the dielectric function of the metal are here represented with $\varepsilon_r(\lambda)$ and $\varepsilon_i(\lambda)$, respectively. When $\varepsilon_i(\lambda)$ is small or only weakly dependent on the wavelength, the wavelength at maximum cross section, λ_{peak}, can be approximated from the resonance condition

$$\varepsilon_r(\lambda_{\text{peak}}) + 2n^2 = 0. \tag{9}$$

It is evident from Eq. (9) that to achieve a large change in λ_{peak} upon changes in the refractive index of the surrounding medium, $\varepsilon_r(\lambda)$ should have a weak wavelength dependence. This condition is met by both gold and silver, which today are the two most commonly used metals in LSPR biosensing applications. Gold and silver also have the additional advantage of having small values of $\varepsilon_i(\lambda)$, which makes the extinction peak sharp. More recently the plasmonic properties of nanoparticles of other metals have also been explored, including aluminum, copper, palladium, and platinum,[45–50] which may provide benefits with respect to fabrication, applicable surface chemistries, or direct use as catalysts.

For nonspherical nanostructures that are significantly smaller than the wavelength of light (the electrostatic limit), the resonance condition for excitation of LSPs can be estimated by introducing a shape factor, χ, into Eq. (9),[21,24]

$$\varepsilon_r(\lambda_{\text{peak}}) + \chi n^2 = 0. \tag{10}$$

For a sphere, χ equals 2, but it is larger for other structures.[21,25] The shape factor will, for example, increase with increasing aspect ratio of gold nanorods, which therefore can be used to tune the peak position of the plasmon resonance.[11,51] For complex nanostructures for which the shape factor cannot be calculated analytically[25] numerical methods, such as the discrete dipole approximation and the finite-difference time domain have proven useful.[7,8,52] Another promising approach to characterize and predict the optical properties of more complex nanostructures, such as nanoshells, nanoeggs, and nanomatryushkas, is the plasmon

hybridization model.[9,10] In this model, complex plasmonic systems are separated into less complex components. After determining the optical properties of the individual components the interactions between them are treated in analogy with the interaction between individual atoms building up molecule. The resulting description of the optical properties of the complex nanostructure is called a hybridized plasmon. For an in-depth presentation of the hybridization model we refer to the work by Prodan *et al.*[10] and Wang *et al.*[9]

A. Sensing with nanoparticles

The first use of the LSPR active nanoparticles in a bioanalytical application was demonstrated ten years ago by Englebienne,[53] who utilized and monitored the color changes in suspended gold colloids induced by changes in the interfacial refractive index caused by antigen-antibody binding events at the interface of the nanoparticles. Thereafter, the concept has been extended to surface-based label-free and real-time studies of biological interactions.[54,55] For example, nanoparticle-based LSPR sensing has been utilized in the investigation of DNA hybridization using immobilized gold colloids,[56] in the detection of biomarkers for Alzheimer disease using nanotriangles made by nanosphere lithography,[4,16] and in the analysis of recombinant protein expression using gold nanoislands.[57] It has also been shown possible to measure spectra from and monitor binding events on single nanoparticles.[58–60] Of particular interest is the fact that the total number of typical protein molecules that can bind to a single nanoscale particle is in the subzeptomole regime ($<10^2$ molecules). This means, in turn, that with a sufficient signal-to-noise ratio ($>10^2$), detection of single binding events may be feasible. Although single-molecule sensitivity was not yet realized, the highest signal-to-noise ratio for measurements on single plasmon active nanostructures obtained so far is, to the best of our knowledge, that by Nusz *et al.* in recording the binding of streptavidin to single biotin-conjugated gold nanorods in real time (see Fig. 5).[61] In this work, the noise level was kept to the minimum by optimizing experimental conditions and monitoring the centroid of the peak (the wavelength corresponding to the center of mass of the peak) instead of the peak position alone, as described by our group in a previous report.[62] The possibility to measure on single nanoparticles and the fact that the LSPR field is, in contrast to the propagating SPR field, spatially confined in all three dimensions opens up for the possibility to develop dense array-based applications and multiplex screening of, for example, immunoreactions and drug candidates using extremely small volumes.

In most cases the bulk sensitivity of LSPR sensors is smaller than that of both prism-coupled and grating-coupled SPR sensors.[55,63–65] However, the decay lengths for the plasmonic fields associated with LSPs are considerably shorter (tens of nanometers) compared to the decay length of SPPs (hundreds of nanometers).[63] Therefore, an adsorbed film of biomolecules (typically <10 nm) will occupy a larger fraction of the total sensing volume of a LSPR sensor compared with a SPR sensor. As a result, the response upon changes in interfacial refractive index due to, e.g., binding of biomolecules to the surface, is comparable for the two sensor concepts. In fact, this makes the two sensor techniques similar in terms of signal-to-noise ratios, which is what eventually determines the detection limit of the sensor in terms of surface coverage. The lowest possible surface coverage that can be measured determines, in turn, the lowest concentration that can be detected because for a reversible reaction, the surface coverage is determined by the affinity constant of the interaction under investigation.

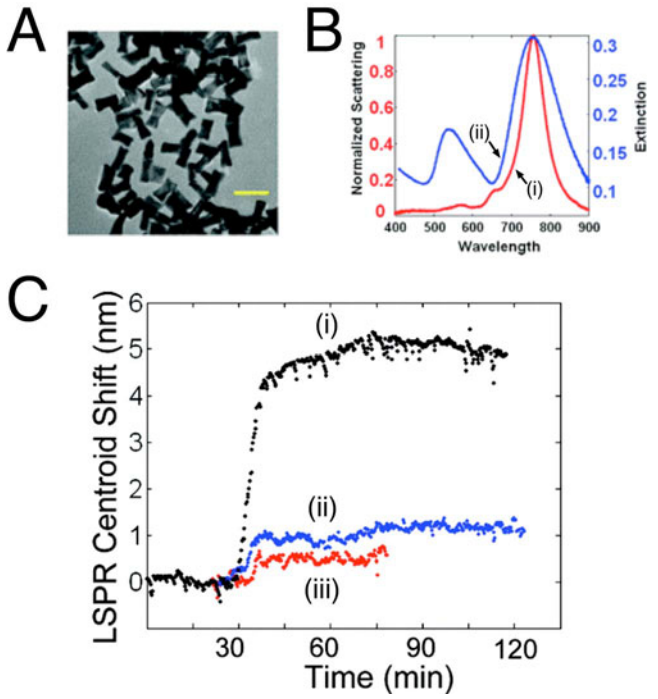

FIG. 5. (A) Transmission electron microscopy image of gold nanorods used for biodetection experiments by Nusz *et al.* (Ref. 61). The scale bar is 100 nm. (B) Scattering spectrum of a single gold nanorod on a glass substrate (i) and the extinction spectrum of an ensemble of gold nanorods suspended in water (ii). (C) Real-time measurement of the LSPR scattering peak centroid shift of single biotin-conjugated gold nanorods incubated in 130 nM (i), 10 nM (ii), and 1 nM (iii) streptavidin in phosphate buffered saline. From Nusz *et al.*, Analytical Chemistry, 2008. Reprinted with permission of American Chemical Society.

High signal-to-noise ratios can be achieved by reducing the noise, as in the center-of-mass based method,[62] but the ratio can also be increased by optimizing the signal obtained in response to a change in interfacial refractive index. Great efforts have been concentrated on means to optimize the sensing properties of nanoparticles by varying primarily their geometries. The shapes presented so far include, but are not limited to, nanodisks,[66] nanoislands,[67] star-shaped particles,[68] nanorice,[14] nanoshells,[69,70] nanorings,[71] and nanocresents.[72,73] In brief, the strive for investigating differently shaped nanostructures can be motivated by inspecting Eq. (10), which shows that the dependence of λ_{peak} on the surrounding refractive index increases with increasing shape factor. Hence, also the bulk sensitivity, S_{bulk}, can be optimized by varying the shape of the nanostructure. To the best of our knowledge, the highest reported value for a

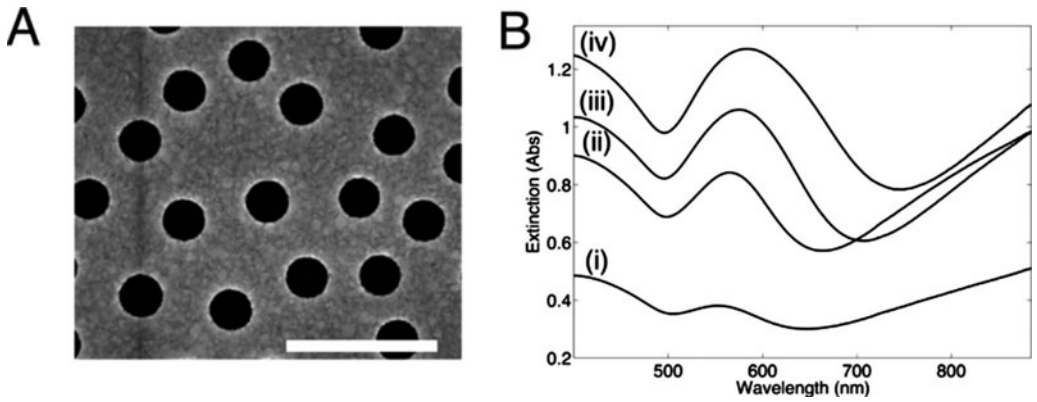

FIG. 6. (A) Scanning electron microscopy image of a typical short-range ordered nanohole sample. The scale bar is 500 nm. (B) Extinction spectra of short-range ordered nanoholes in a gold film with constant aspect ratio and depth and diameter (d:D) corresponding to (i) 30:60 nm, (ii) 55:110 nm, (iii) 70:140 nm, and (iv) 80:160 nm.

nanoparticle-based LSPR structure is 880 nm/RIU for gold nanorings with peak position at around 1500 nm.[74] It is in this context worthwhile to mention that an increase in the bulk sensitivity due to an increase in the shape factor is normally accompanied by an increase in the absolute peak position,[75] which should be taken into consideration in the design of a specific application. For example, it may be important to minimize background absorption and scattering of the light by water, blood, or tissue,[5,61] and many spectrophotometers are also optimized to certain wavelength regions. Also the width of the extinction peak may increase, which is likely to result in less precise determinations of the peak position and hence in increased noise.

In the context of discrete nanoparticles, their potential use in suspensions should also be addressed, such as the pioneering detection schemes invented by Mirkin and co-workers[76,77] based on biorecognition-induced aggregation of nanoparticles resulting in changes in the optical properties visible by the naked eye. In addition, nanoparticles suspended in solution scatter a significant amount of light due to excitation of LSPs, which can be used to determine the position of both monomeric and aggregates of nanoparticles. Recently, this was utilized for intracellular imaging,[3,78] proving the capability of conjugated nanoparticles to be used to successfully differentiate between healthy and cancerous cells.[78] Although beyond the scope of this article, it is also worthwhile to mention that plasmonic nanoparticles are not only promising for the diagnostics of cancer, but also for the treatment of the very same disease.[5] This stems from the fact that absorption of light due to plasmon excitation in nanoparticles is rapidly converted into heat.[79,80] Tissue where nanoparticles have bound/aggregated can therefore be heated locally leading to neutralization of the targeted cells. Of particular interest for both imaging and cancer therapy are plasmonic particles with plasmon resonances in the near-infrared (NIR) region of the wavelength spectrum where the transmission through tissue is high. In this respect, gold nanorods and nanoshells are promising because their plasmon resonances can be tuned into the NIR.[12,79,81] Hirsch *et al.*[82] successfully used this for imaging and photothermal therapy *in vivo* in mice. For the reader interested in plasmonic applications within cancer diagnostics and therapy we refer to the recent review by Jain *et al.*[5]

V. SHORT-RANGE ORDERED NANOHOLES

Similar to discrete nanoparticles, localized plasmon modes have also been associated with a single nanohole in a gold film,[19,83,84] although it has been suggested that the optical phenomena of such a structure essentially is a result from the hole being used as a site for excitation of propagating plasmons.[85] Nevertheless, with respect to biosensing applications it has been shown that the sensitivity of nanoholes positioned in a *short-range order* is highly localized to the void of the nanoholes.[27,86,87] In this context it is worthwhile to point out that because short-range ordered structures lack periodicity, they do not, in contrast to periodic arrays of nanoholes, excite propagating surface plasmons via diffractive coupling.[86] In fact, Prikulis *et al.*[20] showed that short-range ordered nanohole structures have very similar optical behavior to short-range ordered metal nanodisks with identical dimensions. However, the extinction peak was observed to be slightly broader for the nanohole structure, which was attributed to a weak decay channel due to SPPs excited on the perforated metal film. Additional similarities between nanoparticles and short-range ordered nanoholes include that the sensitivity to changes in bulk refractive index is on the same order ($\approx$100 nm/RIU) (Refs. 27, 64, and 83) as is the decay length of the electromagnetic field (tens of nanometers).[83,88]

To investigate the similarities of the optical properties of short-range ordered nanoholes and nanoparticles we have investigated nanoholes with varying depth and diameter. Figure 6 shows a scanning electron microscopy image of a typical short-range ordered nanohole sample and spectra from four different structures with the same aspect ratio of $\frac{1}{2}$ between depth and diameter. As seen in Fig. 6(B) the peak position is approximately the same for all nanohole samples, in agreement with the expectations for excitation of LSPs of nanostructures defined by a unique aspect ratio.[20] Larger val-

ues of the hole size results in much higher extinction values at the peak position, despite the fact that the number of holes per area is significantly reduced. According to Eq. (8) this observation is in agreement with the behavior of nanoparticle plasmons. For the largest holes in Fig. 6(B) (diameter =160 nm), the resonance peak starts to broaden, indicating shortened lifetime of the hole plasmons, potentially due to rapid plasmon decay by radiation, which was also observed and theoretically verified for nanoparticles of comparable sizes.[24,89] All the resonance peaks in Fig. 6(B) are relatively narrow compared to holes with lower aspect ratio (lower depth divided by diameter).[62] Park *et al.*[85] also observed this behavior for single holes and attributed the effect to hybridization of SPP modes at the opposite sides of the metal film. These SPPs make the holes interact at much longer distances than nanoparticles, resulting in a slight blueshift of the plasmon resonance as the distance between holes is decreased for a particular nanohole geometry.[20]

A. Sensing with short-range ordered nanoholes

The fact that the sensing field is localized to the void of short-range ordered nanoholes, together with the decay length being similar to that of nanoparticles,[84,88] suggests that short-range ordered apertures in a thin metal film in most situations provide the same sensing capability as discrete nanoparticles. We therefore refer to sensing with short-range ordered nanoholes as LSPR sensing. This was first utilized by our group using a perforated optically thin gold film supported on glass. In this way, we made use of the ability of lipid vesicles to decompose into planar bilayers on glass to form nanoscale patches of supported lipid bilayers (SLBs) at the bottom of the holes surrounded by gold chemically modified to be inert toward lipid vesicle adsorption. By inserting a small fraction of ganglioside G_{M1} lipids into the planar bilayer patches, this platform was used to detect cholera toxin by recording the colorimetric change of the substrate.[27] Furthermore, due to the dimensions of plasmon active nanostructures, a single macromolecular assembly can be positioned within the hole, given that there is a size match between the macromolecular assembly and the diameter of the hole. In this format, the macromolecular assembly may to a larger extent be located inside the plasmonic field compared to the same molecule attached to a discrete nanoparticle. Based on this insight, we recently reported a scheme for binding of intact lipid vesicles into LSPR active nanoholes in a gold film supported on glass.[86] Vesicles were specifically bound to preformed SLB patches[27] via hybridization of complementary cholesterol-anchored DNA strands, which were self-incorporated into both the SLB patches and into the lipid bilayer of the vesicles.[27,90,91] Thiol-PEG [HS-poly(ethylene glycol)] chemistry was used to passivate the gold surface in order to minimize nonspecific adsorption to regions between the nanoholes. The possibility to bind only one vesicle in each nanohole, which was shown by fluorescence microscopy, together with the possibility to probe single nanoholes,[83] in principle allows single vesicles to be investigated. Of particular interest in this respect is the possibility of probing changes in the refractive index *within* tethered lipid vesicles in response to material transport across the lipid membrane, which was recently proven feasible using conventional SPR.[92] In contrast to, for example, impedance spectroscopy, transport of both charged and noncharged molecules can be monitored, pointing toward a general applicability to studies of transport across cell-membrane mimics.

B. Probing conformational changes with LSPR

The fact that the LSPR field is strongest at and decays rapidly (decay length typically between 10 and 30 nm) away from the surface of a nanoplasmon active structure can be utilized to probe biomolecular structural changes, which was first demonstrated by probing the formation of a SLB from adsorption and subsequent rupture of small lipid vesicles.[64] This was achieved by first coating short-range ordered silver or gold nanoplasmonic hole structures (140 nm in diameter and 30 nm deep) with an approximately 20 nm thick continuous layer of silicon oxide (SiO_x), as depicted schematically in Fig. 7(A). During the rupture process, the lipids that build up the vesicles move toward the sensor surface and thereby into a stronger LSPR field. This conformational change therefore results in a redshift in the LSPR peak position, which can be observed as acceleration in the temporal variation of the plasmon peak position during bilayer formation [see the green curve in Fig. 7(B)]. The potential to utilize shallow LSPR fields to probe conformational changes is not restricted to nanoholes, which was recently demonstrated by Hall *et al.*,[93] who were able to monitor reversible calcium-dependent conformational change in calmodulin using plasmon active arrays of silver nanoprisms. To unambiguously verify that the observed LSPR response can be attributed to a biomacromolecular structural change, we combined the LSPR concept with quartz crystal microbalance with dissipation (QCM-D) monitoring, which is described in Sec. V C.

C. Combined nanoplasmonic and quartz crystal microbalance sensing

A fundamental difference between nanoparticles and nanoholes is that while nanoparticles are discrete, a perforated metal film is continuous and thus electrically conductive. This enables, in the case of nanoholes in metal films, the LSPR concept to be combined with techniques that are based on electrical readout [see schematic in Fig. 7(A)]. Such combinations of sensor concepts are likely to provide the extraction of additional information about the studied systems that is not accessible with the single techniques alone. We recently developed a combination of the LSPR method with the QCM-D monitoring,[88,94] which relied on the fact that a plasmon active short-range ordered nanohole surface can be used as one of the electrodes of a QCM crystal. To form a supported lipid bilayer on the surface, the same structure as described above was used (~20 nm SiO_x sputtered on the short-range ordered gold nanoholes). Because the QCM-D technique provides characteristic signatures for the structural changes that occur during spontaneous SLB formation from

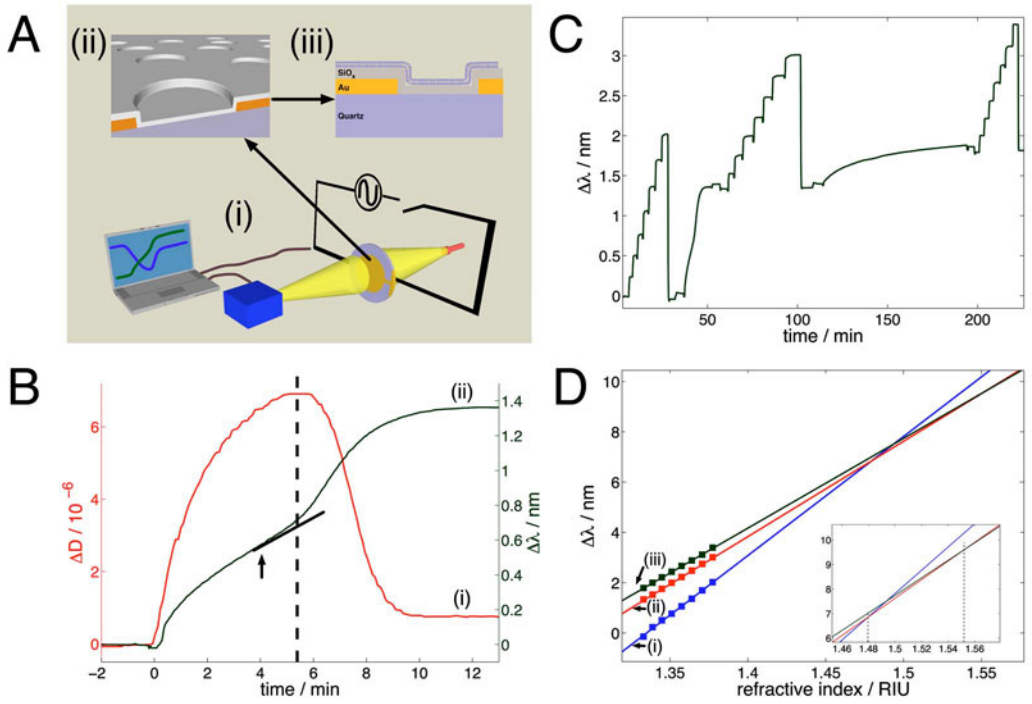

FIG. 7. (A) Schematic illustration of the combined QCM-D and LSPR sensor setup. (i) The flashlight and the blue box represent the light source and the spectrometer, respectively. The electric circuit represents a simplified version of the QCM readout system, which, just as the spectrometer, is connected to a computer. (ii) A schematic illustration depicting a small area of the sensor surface. (iii) Illustration of the cross section through a nanohole after bilayer formation. (Not drawn to scale) (B) Temporal variation in the dissipation, ΔD, (i) and the LSPR peak position, $\Delta\lambda$, (ii) during bilayer formation on the nanostructured surface. The vertical dashed line is there as a visual aid and to demonstrate the temporal correlation between the turnover in the dissipation and the LSPR kink, respectively. The short line and the arrow demonstrate the possibility to investigate the initiation of vesicle rupture from the LSPR response. (C) Temporal variations of the peak position, $\Delta\lambda$, due to the following sequential steps: (1) bulk sensitivity measurement using increasing concentrations of glycerol, (2) bilayer formation from lipid vesicles, (3) bulk sensitivity measurement, (4) adsorption of NeutrAvidin to the functionalized bilayer, and (5) bulk sensitivity measurement. (D) The peak shift versus the refractive index for the experimental values (squares) extracted from (C) for the glycerol cycle before (i), after bilayer formation (ii) and after adsorption of NeutrAvidin (iii). The full lines are linear fits to the experimental data. The inset is a close up of the same graph and the dashed lines mark the intersections that represent the refractive index of the SLB and NeutrAvidin, respectively. From Jonsson *et al.*, Analytical Chemistry, 2008. Reprinted with permission of American Chemical Society.

lipid vesicle adsorption on silica,[95] the combined setup therefore provides independent responses that are sensitive to conformational changes. However, while the LSPR signal is most sensitive to processes that occur inside the nanoholes, the contribution to the QCM-D response will be dominated by binding reactions on the planar regions between the nanoholes. Hence, the excellent temporal correlation between the two signatures attributed to bilayer formation [Fig. 7(B)] therefore implies that the rupture of vesicles is initiated at the approximate same time inside and between nanoholes. This example thus illustrates a unique possibility provided by an electrically conductive LSPR active substrate, pointing toward future combinations with, for example, electrochemistry, which was already proven valuable in combination with propagating SPR,[96] as well as impedance spectroscopy, which is an important tool in studies of, for example, supported cell-membrane mimics.[97]

D. Quantification of the sensor response from LSPR measurements

An aspect of outmost importance for any bioanalytical tool is the ability to make quantitative estimates of the physical properties of the analyzed entities, including the number of detected molecules. An important aspect of LSPR sensors is that they provide the possibility to estimate the absolute refractive index of adsorbed molecules by simply performing bulk sensitivity measurements before and after the adsorption process. This concept was first used by Haes *et al.*[98] to determine the absolute refractive index of hexadecanethiols adsorbed on silver nanoparticles. The principle is exemplified in Fig. 7, showing linear fits [Fig. 7(D)] corresponding to sensitivity measurements prior to (blue) and after (red) the supported lipid bilayer formation described above and also after additional adsorption of NeutrAvidin to the biotinylated SLB (green). Note that the bulk sensitivity curves are separated (at the refractive index of the buffer) by the LSPR shift induced by the adsorption processes [Fig. 7(D)]. As seen, the separations of the linear extrapolations decrease with increasing refractive index and, consequently, the refractive indices at which the two pairs of curves (blue/red and red/green) coincide, correspond to the *absolute* refractive indices of the SLB and the protein, respectively.[88] The possibility of using this approach to determine the absolute refractive index of the bound molecules originates from the shallow evanescent fields associated with nanoplasmon active substrates, which, in contrast to conventional SPR, means that a thin

film (<5 nm) will already occupy a substantial fraction of the sensing volume. Note, in particular, that this determination of the absolute refractive index requires no assumptions regarding the spatial distribution of the electromagnetic field.

Under the assumption that the evanescent field decays exponentially, which has been shown a sufficiently good approximation even in cases of irregular nanoparticles,[84,99,100] the decay length can be estimated from the blue and red sensitivity curves in Fig. 7(D), given that the thickness of the molecular film (supported lipid bilayer in this case) is known. Fortunately, in the combined QCM-D/LSPR setup the thickness is obtained from the QCM-D response and for short-range ordered gold nanoholes (140 nm in diameter, 30 nm deep,20 nm SiO_x) the decay length of the field intensity (twice that of the field strength), L, could be determined to approximately 20 nm, which is in good agreement with other reports.[83] Following the analysis for conventional SPR sensors introduced by Jung *et al.*[65] the expected peak shift, $\Delta\lambda_{peak}$, induced by a molecular film with thickness t and *effective* refractive index n_{film} can be obtained from

$$\Delta\lambda_{peak} = S_{bulk}(n_{film} - n_{buffer})(1 - e^{-t/L}), \tag{11}$$

where S_{bulk} is the bulk sensitivity and n_{buffer} is the refractive index of the surrounding buffer solution. Hence, with the thickness of the film and the decay length of the LSPR field known, the effective film refractive index can be determined. This, in turn, can be used to estimate the adsorbed mass per area on the surface according to the Lorentz–Lorenz relation[101,102]

$$\Delta m_{LSPR} = 3t(n_{film} - n_{buffer}) \times \frac{(n_{film} + n_{buffer})}{(n_{film}^2 + 2)[r(n_{buffer}^2 + 2) - \nu(n_{buffer}^2 - 1)]}, \tag{12}$$

where r and ν are the specific refractivity and the specific volume (inverse of the density) of the adsorbed molecules, respectively. Note also that the specific refractivity can be determined from the absolute refractive index, $n_{molecule}$, of the molecules as

$$r = \nu\frac{n_{molecule}^2 - 1}{n_{molecule}^2 + 2}. \tag{13}$$

This, in turn, means that we are left with two unknowns: the specific volume (or the density) which is generally a known parameter, and the thickness, which in the example above was obtained from simultaneous QCM-D measurements.[88] It is emphasized, however, that the thickness can generally be estimated from the molecular dimension of the adsorbed entities, and if smaller than the decay length of the evanescent field, an error in the thickness determination leads to an at least twofold lower error in the mass determination. Hence, we propose this method, based on bulk sensitivity measurements prior to and after the adsorption reactions, as a generic way of calibrating arbitrary nanoplasmonic sensors for mass-uptake estimations.

VI. CONCLUDING REMARKS

Based on numerous examples, whereof we have only highlighted a brief selection in this article, nanoplasmonics have proven valuable in bioanalytical applications, and we strongly believe that their use in biological and medical research will evolve into an even more important component in the near future. Regarding refractive index based sensing, we have presented a generic means to quantify the bound molecular mass, which is expected to be accurate to within at least 10%. However, complete theoretical descriptions of the electromagnetic fields associated with, e.g., short-range ordered nanoholes will still be extremely valuable, for example, in the analysis of optical responses associated with biomolecular structural changes, where nanoplasmonics provide a unique means to study such phenomena without the introduction of external labels. Especially when synchronized with techniques providing alternative information, here exemplified with QCM-D measurements, we expect this feature to become one of the most valuable merits of nanoplasmonic sensors. This, in combination with the possibility to record the response of down to single nanostructures, may very well open up entirely new avenues in this and related fields of research. It should also be emphasized that apart from the refractive index based sensing addressed herein, the plasmon properties associated with nanostructures also provide other biologically relevant applications, such as those based on plasmon-enhanced fluorescence[103,104] and surface enhanced Raman scattering.[105–108] Common for all these applications is that optimal performance relies on the ability to fine tune the structure, composition, and surface chemistry at the nanoscale level, and although significant progress has been achieved during the past decade, we are convinced that we have only seen the beginning.

ACKNOWLEDGMENTS

This work was financially supported by the Swedish Research Council, the Biomimetic, Ingvar and BioNanoIT programs funded by SSF and Vinnova.

[1]C. Hagglund, M. Zach, G. Petersson, and B. Kasemo, Appl. Phys. Lett. **92**, 053110 (2008).
[2]H. A. Atwater, Sci. Am. **296**, 56 (2007).
[3]S. Kumar, N. Harrison, R. Richards-Kortum, and K. Sokolov, Nano Lett. **7**, 1338 (2007).
[4]A. J. Haes, L. Chang, W. L. Klein, and R. P. Van Duyne, J. Am. Chem. Soc. **127**, 2264 (2005).
[5]P. K. Jain, I. H. El-Sayed, and M. A. El-Sayed, Nanotoday **2**, 18 (2007).
[6]Y. Chen and A. Pepin, Electrophoresis **22**, 187 (2001).
[7]B. T. Draine, and P. J. Flatau, J. Opt. Soc. Am. A **11**, 1491 (1994).
[8]M. Futamata, Y. Maruyama, and M. Ishikawa, J. Phys. Chem. B **107**, 7607 (2003).
[9]E. Prodan, C. Radloff, N. J. Halas, and P. Nordlander, Science **302**, 419 (2003).
[10]H. Wang, D. W. Brandl, P. Nordlander, and N. J. Halas, Acc. Chem. Res. **40**, 53 (2007).
[11]B. Nikoobakht and M. A. El-Sayed, Chem. Mater. **15**, 1957 (2003).
[12]S. J. Oldenburg, R. D. Averitt, S. L. Westcott, and N. J. Halas, Chem. Phys. Lett. **288**, 243 (1998).
[13]Y. G. Sun and Y. N. Xia, Science **298**, 2176 (2002).
[14]H. Wang, D. W. Brandl, F. Le, P. Nordlander, and N. J. Halas, Nano Lett. **6**, 827 (2006).

[15]P. Hanarp, D. S. Sutherland, J. Gold, and B. Kasemo, Colloids Surf., A **214**, 23 (2003).
[16]J. C. Hulteen and R. P. van Duyne, J. Vac. Sci. Technol. A **13**, 1553 (1995).
[17]A. Dmitriev, T. Pakizeh, M. Kall, and D. S. Sutherland, Small **3**, 294 (2007).
[18]H. Wei, U. Håkansson, Z. Yang, F. Höök, and H. Xu, Small **4**, 1296 (2008).
[19]A. Degiron, H. J. Lezec, N. Yamamoto, and T. W. Ebbesen, Opt. Commun. **239**, 61 (2004).
[20]J. Prikulis, P. Hanarp, L. Olofsson, D. Sutherland, and M. Kall, Nano Lett. **4**, 1003 (2004).
[21]M. E. Stewart, C. R. Anderton, L. B. Thompson, J. Maria, S. K. Gray, J. A. Rogers, and R. G. Nuzzo, Chem. Rev. (Washington, D.C) **108**, 494 (2008).
[22]C. Genet and T. W. Ebbesen, Nature (London) **445**, 39 (2007).
[23]J. Homola, Chem. Rev. (Washington, D.C) **108**, 462 (2008).
[24]P. K. Jain, X. Huang, I. H. El-Sayed, and M. A. El-Sayad, Plasmonics **2**, 107 (2007).
[25]K. A. Willets and R. P. Van Duyne, Annu. Rev. Phys. Chem. **58**, 267 (2007).
[26]A. G. Brolo, R. Gordon, B. Leathem, and K. L. Kavanagh, Langmuir **20**, 4813 (2004).
[27]A. Dahlin, M. Zach, T. Rindzevicius, M. Kall, D. S. Sutherland, and F. Hook, J. Am. Chem. Soc. **127**, 5043 (2005).
[28]G. Rong, H. Wang, L. R. Skewis, and B. M. Reinhard, Nano Lett.. **8**, 338 (2008).
[29]J. Homola, S. S. Yee, and G. Gauglitz, Sens. Actuators B **54**, 3 (1999).
[30]B. Liedberg, C. Nylander, and I. Lundstrom, Sens. Actuators **4**, 299 (1983).
[31]E. Kretschmann and H. Raether, Z. Naturforsch. A **23**, 2135 (1968).
[32]I. D. Alves, C. K. Park, and V. J. Hruby, Current Protein & Peptide Science **6**, 293 (2005).
[33]B. Rothenhausler and W. Knoll, Nature (London) **332**, 615 (1988).
[34]T. Liebermann and W. Knoll, Colloids Surf., A **171**, 115 (2000).
[35]J. Dostalek and J. Homola, Sens. Actuators B **129**, 303 (2008).
[36]R. H. Ritchie, E. T. Arakawa, J. J. Cowan, and R. N. Hamm, Phys. Rev. Lett. **21**, 1530 (1968).
[37]T. W. Ebbesen, H. J. Lezec, H. F. Ghaemi, T. Thio, and P. A. Wolff, Nature (London) **391**, 667 (1998).
[38]H. F. Ghaemi, T. Thio, D. E. Grupp, T. W. Ebbesen, and H. J. Lezec, Phys. Rev. B **58**, 6779 (1998).
[39]M. E. Stewart *et al.*, Proc. Natl. Acad. Sci. U.S.A. **103**, 17143 (2006).
[40]W. L. Barnes, A. Dereux, and T. W. Ebbesen, Nature (London) **424**, 824 (2003).
[41]A. Krishnan *et al.*, Opt. Commun. **200**, 1 (2001).
[42]J. M. Yao, M. E. Stewart, J. Maria, T. W. Lee, S. K. Gray, J. A. Rogers, and R. G. Nuzzo, Angew. Chem., Int. Ed. **47**, 5013 (2008).
[43]A. Degiron and T. W. Ebbesen, J. Opt. A, Pure Appl. Opt. **7**, S90 (2005).
[44]G. Mie, Ann. Phys. **25**, 330 (1908).
[45]G. H. Chan, J. Zhao, E. M. Hicks, G. C. Schatz, and R. P. Van Duyne, Nano Lett. **7**, 1947 (2007).
[46]G. H. Chan, J. Zhao, G. C. Schatz, and R. P. V. Duyne, J. Phys. Chem. C **112**, 13958 (2008).
[47]C. Langhammer, B. Kasemo, and I. Zoric, J. Chem. Phys. **126**, 194702 (2007).
[48]C. Langhammer, M. Schwind, B. Kasemo, and I. Zoric, Nano Lett. **8**, 1461 (2008).
[49]C. Langhammer, Z. Yuan, I. Zoric, and B. Kasemo, Nano Lett. **6**, 833 (2006).
[50]C. Langhammer, I. Zoric, and B. Kasemo, Nano Lett. **7**, 3122 (2007).
[51]S. Link, M. B. Mohamed, and M. A. El-Sayed, J. Phys. Chem. B **103**, 3073 (1999).
[52]C. Oubre and P. Nordlander, J. Phys. Chem. B **108**, 17740 (2004).
[53]P. Englebienne, Analyst (Cambridge, U.K.) **123**, 1599 (1998).
[54]G. Kalyuzhny, A. Vaskevich, M. A. Schneeweiss, and I. Rubinstein, Chem.-Eur. J. **8**, 3850 (2002).
[55]N. Nath and A. Chilkoti, Anal. Chem. **74**, 504 (2002).
[56]L. Olofsson, T. Rindzevicius, I. Pfeiffer, M. Kall, and F. Hook, Langmuir **19**, 10414 (2003).
[57]Y.-B. Shin, J.-M. Lee, M.-R. Park, M.-G. Kim, B. H. Chung, H.-B. Pyo, and S. Maeng, Biosens. Bioelectron. **22**, 2301 (2007).
[58]J. J. Mock, M. Barbic, D. R. Smith, D. A. Schultz, and S. Schultz, J. Chem. Phys. **116**, 6755 (2002).
[59]A. D. McFarland and R. P. Van Duyne, Nano Lett. **3**, 1057 (2003).
[60]G. Raschke, S. Kowarik, T. Franzl, C. Sonnichsen, T. A. Klar, J. Feldmann, A. Nichtl, and K. Kurzinger, Nano Lett. **3**, 935 (2003).
[61]G. J. Nusz, S. M. Marinakos, A. C. Curry, A. Dahlin, F. Hook, A. Wax, and A. Chilkoti, Anal. Chem. **80**, 984 (2008).
[62]A. B. Dahlin, J. O. Tegenfeldt, and F. Hook, Anal. Chem. **78**, 4416 (2006).
[63]A. J. Haes and R. P. Van Duyne, Anal. Bioanal. Chem. **379**, 920 (2004).
[64]M. P. Jonsson, P. Jonsson, A. B. Dahlin, and F. Hook, Nano Lett. **7**, 3462 (2007).
[65]L. S. Jung, C. T. Campbell, T. M. Chinowsky, M. N. Mar, and S. S. Yee, Langmuir **14**, 5636 (1998).
[66]P. Hanarp, M. Kall, and D. S. Sutherland, J. Phys. Chem. B **107**, 5768 (2003).
[67]I. Doron-Mor, H. Cohen, Z. Barkay, A. Shanzer, A. Vaskevich, and I. Rubinstein, Chem.-Eur. J. **11**, 5555 (2005).
[68]C. L. Nehl, H. W. Liao, and J. H. Hafner, Nano Lett. **6**, 683 (2006).
[69]R. D. Averitt, D. Sarkar, and N. J. Halas, Phys. Rev. Lett. **78**, 4217 (1997).
[70]Y. G. Sun and Y. N. Xia, Anal. Chem. **74**, 5297 (2002).
[71]J. Aizpurua, P. Hanarp, D. S. Sutherland, M. Kall, G. W. Bryant, and F. J. G. de Abajo, Phys. Rev. Lett. **90**, 057401 (2003).
[72]R. Bukasov and J. S. Shumaker-Parry, Nano Lett. **7**, 1113 (2007).
[73]J. S. Shumaker-Parry, H. Rochholz, and M. Kreiter, Adv. Mater. (Weinheim, Ger.) **17**, 2131 (2005).
[74]E. M. Larsson, J. Alegret, M. Kall, and D. S. Sutherland, Nano Lett. **7**, 1256 (2007).
[75]M. M. Miller and A. A. Lazarides, J. Phys. Chem. B **109**, 21556 (2005).
[76]C. A. Mirkin, R. L. Letsinger, R. C. Mucic, and J. J. Storhoff, Nature (London) **382**, 607 (1996).
[77]N. L. Rosi and C. A. Mirkin, Chem. Rev. (Washington, D.C) **105**, 1547 (2005).
[78]I. H. El-Sayed, X. Huang, and M. A. El-Sayed, Nano Lett. **5**, 829 (2005).
[79]M. A. El-Sayed, Acc. Chem. Res. **34**, 257 (2001).
[80]S. Link and M. A. El-Sayed, J. Phys. Chem. B **103**, 8410 (1999).
[81]C. J. Murphy, T. K. San, A. M. Gole, C. J. Orendorff, J. X. Gao, L. Gou, S. E. Hunyadi, and T. Li, J. Phys. Chem. B **109**, 13857 (2005).
[82]L. R. Hirsch *et al.*, Proc. Natl. Acad. Sci. U.S.A. **100**, 13549 (2003).
[83]T. Rindzevicius, Y. Alaverdyan, A. Dahlin, F. Hook, D. S. Sutherland, and M. Kall, Nano Lett. **5**, 2335 (2005).
[84]T. Rindzevicius, Y. Alaverdyan, B. Sepulveda, T. Pakizeh, M. Kall, R. Hillenbrand, J. Aizpurua, and F. J. G. de Abajo, J. Phys. Chem. C **111**, 1207 (2007).
[85]T. H. Park, N. Mirin, J. B. Lassiter, C. L. Nehl, N. J. Halas, and P. Nordlander, ACS Nano **2**, 25 (2008).
[86]A. B. Dahlin, M. P. Jonsson, and F. Höök, Adv. Mater. (Weinheim, Ger.) **20**, 1436 (2008).
[87]R. Marie, A. B. Dahlin, J. O. Tegenfeldt, and F. Hook, Biointerphases **2**, 49 (2007).
[88]M. P. Jonsson, P. Jönsson, and F. Höök, Anal. Chem. **80**, 7988 (2008).
[89]K. S. Lee and M. A. El-Sayed, J. Phys. Chem. B **110**, 19220 (2006).
[90]I. Pfeiffer and F. Hook, J. Am. Chem. Soc. **126**, 10224 (2004).
[91]S. Svedhem, I. Pfeiffer, C. Larsson, C. Wingren, C. Borrebaeck, and F. Hook, ChemBioChem **4**, 339 (2003).
[92]M. Brandén, S. Forsvall, and F. Hook, ChemPhysChem, DOI: 10.1002/cphc.200800614.
[93]W. P. Hall, J. N. Anker, Y. Lin, J. Modica, M. Mrksich, and R. P. Van Duyne, J. Am. Chem. Soc. **130**, 5836 (2008).
[94]A. B. Dahlin, P. Jonsson, M. P. Jonsson, E. Schmid, and F. Hook, ACS Nano **2**, 2174 (2008).
[95]C. A. Keller and B. Kasemo, Biophys. J. **75**, 1397 (1998).
[96]R. J. Heaton, A. W. Peterson, and R. M. Georgiadis, Proc. Natl. Acad. Sci. U.S.A. **98**, 3701 (2001).
[97]C. Steinem, A. Janshoff, W. P. Ulrich, M. Sieber, and H. J. Galla, Biochim. Biophys. Acta **1279**, 169 (1996).
[98]A. J. Haes, S. L. Zou, G. C. Schatz, and R. P. Van Duyne, J. Phys. Chem. B **108**, 6961 (2004).
[99]A. J. Haes, S. L. Zou, G. C. Schatz, and R. P. Van Duyne, J. Phys. Chem. B **108**, 109 (2004).
[100]Y. Zhou, H. Xu, A. B. Dahlin, J. Vallkil, C. A. K. Borrebaeck, C. Wingren, B. Liedberg, and F. Hook, Biointerphases **2**, 6 (2007).
[101]P. A. Cuypers, J. W. Corsel, M. P. Janssen, J. M. Kop, W. T. Hermens, and

H. C. Hemker, J. Biol. Chem. **258**, 2426 (1983).
[102]E. Reimhult, C. Larsson, B. Kasemo, and F. Hook, Anal. Chem. **76**, 7211 (2004).
[103]A. G. Brolo, S. C. Kwok, M. G. Moffitt, R. Gordon, J. Riordon, and K. L. Kavanagh, J. Am. Chem. Soc. **127**, 14936 (2005).
[104]I. Gryczynski, J. Malicka, Y. B. Shen, Z. Gryczynski, and J. R. Lakowicz, J. Phys. Chem. B **106**, 2191 (2002).
[105]J. B. Jackson and N. J. Halas, Proc. Natl. Acad. Sci. U.S.A. **101**, 17930 (2004).
[106]D. L. Jeanmaire and R. P. Van Duyne, J. Electroanal. Chem. Interfacial Electrochem. **84**, 1 (1977).
[107]S. M. Nie and S. R. Emery, Science **275**, 1102 (1997).
[108]S. J. Oldenburg, S. L. Westcott, R. D. Averitt, and N. J. Halas, J. Chem. Phys. **111**, 4729 (1999).